ACCOUNTS
of chemical research

# Surface Structure at the Ionic Liquid–Electrified Metal Interface

STEVEN BALDELLI
*Department of Chemistry, University of Houston, Houston, Texas 77204-5003*

RECEIVED ON AUGUST 9, 2007

## CONSPECTUS

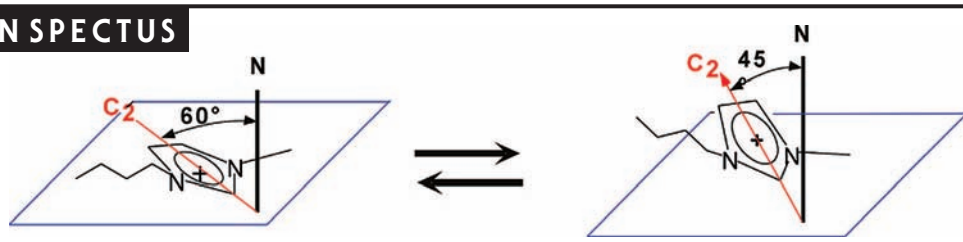


Room-temperature ionic liquids are a new class of liquids with many important uses in electrical and electrochemical devices. The liquids are composed purely of ions in the liquid state with no solvent. They generally have good electrical and ionic conductivity and are electrochemically stable. Since their applications often depend critically on the interface structure of the liquid adjacent to the electrode, a molecular level description is necessary to understanding and improving their performance.

There are currently no adequate models or descriptions on the organization of the ions, in these pure ionic compounds, adjacent to the electrode surface. In normal electrolytic solutions, the organization of solvent and ions is adequately described by the Gouy–Chapman–Sterns model. However, this model is based on the same concepts as those in Debye–Huckel theory, that is a dilute electrolyte, where ions are well-separated and noninteracting. This is definitely not the situation for ionic liquids. Thus our goal was to investigate the ionic liquid–metal interface using surface-specific vibrational spectroscopy sum frequency generation, SFG. This technique can probe the metal–liquid interface without interference from the bulk electrolyte. Thus the interface is probed in situ while the electrode potential is changed. To compliment the vibrational spectroscopy, electrochemical impedance spectroscopy (EIS) is used to measure the capacitance and estimate the "double layer" thickness and the potential of zero charge (PZC). In addition, the vibrational Stark shift of CO adsorbed on the Pt electrode was measured to provide an independent measure of the "double layer" thickness. All techniques were measured as a function of applied potential to provide full description of the interface for a variety of imidazolium-based (cation) ionic liquids.

The vibrational Stark shift and EIS results suggest that ions organize in a Helmholtz-like layer at the interface, where the potential drop occurs over the a range of 3–5 Å from the metal surface into the liquid. Further, the SFG results imply that the "double layer" structure is potential-dependent; At potentials positive of the PZC, anions adsorbed to the surface and the imidazolium ring are repelled to orient more along the surface normal, compared with the potentials negative of the PZC, at which the cation is oriented more parallel to the surface plane and the anions are repelled from the surface.

The results present a view of the ionic liquid–metal electrode interface having a very thin "double layer" structure where the ions form a single layer at the surface to screen the electrode charge. However, the results also raise many other fundamental questions as to the detailed nature of the interfacial structure and interpretations of both electrochemical and spectroscopic data.

There has been a large growth in the electrochemical applications and investigations[1–3] on ionic liquids. They are utilized as electrolytes in batteries,[3–5] fuel cells,[3,6–8] super capacitors,[3,9–11] solar cells,[12–15] devices,[16,17] and electrochemical reactions.[18,19] Despite this increase, models describing the arrangement of ions at the interface of an ionic liquid and an electrode are insufficient. This Account discusses the use of molecular-level spectroscopic techniques in com-

Published on the Web 01/31/2008 www.pubs.acs.org/acr
10.1021/ar700185h CCC: $40.75 

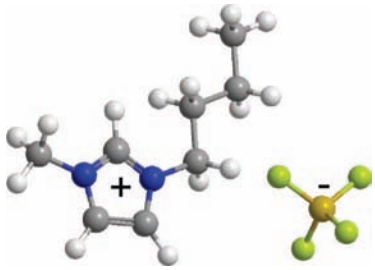

**FIGURE 1.** Structure of 1-butyl-3-methylimidazolium tetrafluoroborate, [BMIM][$BF_4$].

bination with electrochemical methods to deduce the structure of ionic liquids at the electrochemical interface.

Room-temperature ionic liquids are typically composed of organic cations and either organic or inorganic anions.[20]

The structure of a common room-temperature ionic liquid based on alkyl imidazolium is given in Figure 1. The first-order description of ionic liquids is that they are simple charged species in a liquid state. While Coulombic interactions are the dominant force between the ions, the ions are not simply spheres of charge but have shape and chemical functionality that impose subtle changes in the physical properties. Thus, dipole, hydrogen-bonding, and dispersive forces are important to the interactions between constituents in the ionic liquid;[21,22] however, these forces are weak enough to keep them liquid at room temperature. They have a high thermal stability, wide electrochemical window, and very low vapor pressure. These properties and others are modified by the variation in the ionic liquid composition. It must be emphasized that ionic liquids are not ions in solution but are pure compounds and they are conceptually similar to $Na^+Cl^-$(l) not $Na^+Cl^-$(aq). As NaCl melts at 800 °C, [BMIM][$BF_4$] melts at approximately −50 °C. This pure ionic character gives them unusual properties compared with electrolytic solutions or polar organic solvents.

Our purpose is to explore the consequences of a pure electrolyte at the interface in an electrochemical system. We are interested in how a solvent-less ionic medium will structure and arrange at the interface. How will the ions respond to the changes in the surface charge or potential or in the ionic liquid composition? The electrochemical system is particularly important since it is a major application of ionic liquids. In addition, electrochemical techniques are applicable to the system and used to control and measure the macroscopic properties at the interface.

The description of electrolytic solution structure at an interface is a classic, highly investigated system due to its ubiquitous occurrence in nature and technology.[23–26] However, pure electrolytes are much less studied.[23,27–32] There are three limiting cases to describe the charge distribution of an ion near an interface. These are the Helmholtz model, the Gouy–Chapman model, and the layer model as represented in Figure 2. It is noted that all three, or combinations of them, have been proposed in the description of the ionic liquid/molten salt–metal interface. Traditionally, these models are distinguished by their capacitance, which is then used to evaluate the charge or potential distribution at the surface. Consequently, the double layer is discussed in terms of a distance or thickness analogous to a parallel plate capacitor.

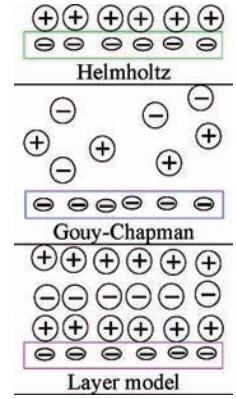


**FIGURE 2.** Three common models for the electrochemical interface.

The Helmholtz model is one of the original models used to describe charges at a boundary. The term "electrical double layer" originates from this model, since the charge on the electrode is balanced by a single layer of counter charge from the liquid. Equation 1 shows the simple form of the capacitance.

$$\frac{1}{C_d} = \frac{d}{\epsilon\epsilon_0} \tag{1}$$

where $C_d$ is the double layer capacitance, $\epsilon_0$ is the permittivity of vacuum, and $\epsilon$ is the relative permittivity. The distance, $d$, is the range over which the potential drop occurs.[26]

The most popular model is the Gouy–Chapmann double layer. In this description, the ions form a diffuse layer of charge segregation at the interface. That is, the counter charge is spread through the solution adjacent to the electrode up to a few nanometers depending on the ions, solvent, and ion concentration. Thus, the capacitance takes a more complicated form:[33]

$$\frac{1}{C_d} = \left(\frac{2\epsilon\epsilon_0 z^2 e^2 n^0}{kT}\right)^{-1/2} \frac{1}{\cosh\left(\frac{ze\varphi_0}{2kT}\right)} \tag{2}$$

Here $\varphi_0$ is the potential and $n^0$ is the ion number density, the rest of the symbols having their usual meaning.[33] Further, it

is derived from a Debye−Huckel approximation of dilute electrolytic solution, which seems unlikely for the ionic liquid system. However, some features of Gouy−Chapman, especially the capacitance−voltage ($C-V$) dependence could be important. A representation of this structure is also given in Figure 2. It should be noted that often a combination of the Helmholtz and Gouy−Chapman models is given as a Gouy−Chapman−Sterns (GCS) model.

Finally, it has been proposed that ions, especially in molten salts, form layer structures at the electrode interface. This model seems reasonable given the large Coulombic forces and since the layering resembles a lattice from which the liquid is derived. The capacitance response for this situation has been derived for molten salts and is given in eq 3.[30]

$$\frac{1}{C_d} = \frac{1}{C_k} - \frac{\delta}{\epsilon_0\left(1 - \frac{\delta\beta|\xi|}{\epsilon_0}\right)} \quad (3)$$

where $\xi$ is the charge density on the metal, $C_k = \epsilon\epsilon_0/d$ is the capacitance of a parallel plate capacitor where $d$ is the cation radius, and $\delta^2 = (2\epsilon_0 kT)/(q^2 c_0(z-2))$ and $\beta = (\alpha q c_0(z-1))/(2\epsilon_0 kT)$ are functions of the concentration of vacancies $c_0$, the coordination number $z$, the charge of vacancy $q$, and the polarizability, $\alpha$. The model produced fair agreement with experiments on molten salts but has not been thoroughly tested on ionic liquids.[32]

The goal of this research is to use electrical and spectroscopic measurements to elucidate the structure of the ionic liquid−electrode interface. The use of these distinct methods converges to provide a consistent view on the arrangement of ions at a room- temperature ionic liquid−electrified metal interface. For example, electrochemistry supplies information on the thickness of the interface, while sum frequency generation (SFG) provides the direct chemical information on the functional groups at the surface and how they are oriented.

SFG is an important technique to the investigation of electrochemical interfaces[34−36] because chemically and spectroscopically, molecules in the bulk solution are barely distinguishable from those adjacent to the electrode. However, at the interface, molecules tend to be in a noncentrosymmetric environment (i.e., slightly aligned) and thus are effectively probed with nonlinear optical techniques that rely on a coherent $\chi^{(2)}$ process. In the electric dipole approximation, a $\chi^{(2)}$ process is allowed in environments without inversion symmetry but $\chi^{(2)} = 0$ in centrosymmetric media, such as the bulk liquid.[37,38] Thus, SFG is a very valuable technique to probe the electrochemical interface.[34] SFG has several other useful properties besides its surface specificity.

$$I_{SF} \propto |\overleftrightarrow{\chi}^{(2)}{:}E_{vis}E_{IR}|^2 \quad (4)$$

It provides a vibrational spectrum of the interfacial molecules giving a molecular-level description of the surface. In addition, by using polarized input beams and analyzing the polarization state of the output, the orientation of the molecules is estimated.

$$\chi^{(2)} = \chi^{(2)}_R + \chi^{(2)}_{NR} = \sum_q \frac{NA_q}{\omega IR - \omega q + i\Gamma} + \chi^{(2)}_{NR} \quad (5)$$

Finally, SFG is able to provide good temporal[39,40] and spatial resolution of the interface.[41−44]

SFG spectroscopy involves the overlap of a visible laser beam with a frequency-tunable infrared beam at the surface. Intense SF signal is generated as the IR matches the vibrational resonance of an interfacial molecule as illustrated in eqs 4 and 5.

A diagram of a picosecond-scanning SFG spectrometer, which is used at the University of Houston, is shown in Figure 3.[45] The system is capable of scanning from 1000 to 4000 $cm^{-1}$. An important feature of this spectrometer is the presence of a reference arm used for normalizing the SFG spectra. Since the SF signal depends on the input intensity of the IR and visible beams (see eq 4) it is critical to correct the SFG spectra for their variation. Typically the IR will vary significantly over the course of a spectral scan due to the changing efficiency of the OPG/OPA (IR source) and by absorption as the IR passes through the bulk liquid in the SFG cell (see below). To account for both effects, the IR light that is reflected from the electrode surface is mixed with residual 532 nm light in a nonlinear crystal where the SFG reference intensity varies as a function of the IR intensity. SFG from the reference channel is collected simultaneously with each data point to provide an accurate and sensitive correction.[34]

In the beginning of this project, a variety of clean, affordable ionic liquids were not commercially available, and for surface chemistry, purity is critical. There are four criteria used to evaluate the ionic liquid quality: color, halide concentration, water concentration, and H and C NMR quality. All the ionic liquids used in these studies, which are based on alkyl imidazolium cations and simple anions, are completely colorless and transparent. Further, the cyclic voltammetry must be stable over 3−6 V, depending on the ions, and the NMR must correspond to the compound synthesized with no additional peaks. The ionic liquids used in the group are synthesized and purified to meet these criteria. Similarly, once clean ionic liquids are created, they must be handled in an uncontaminated reliable fashion into the spectroscopy cell. This involved the

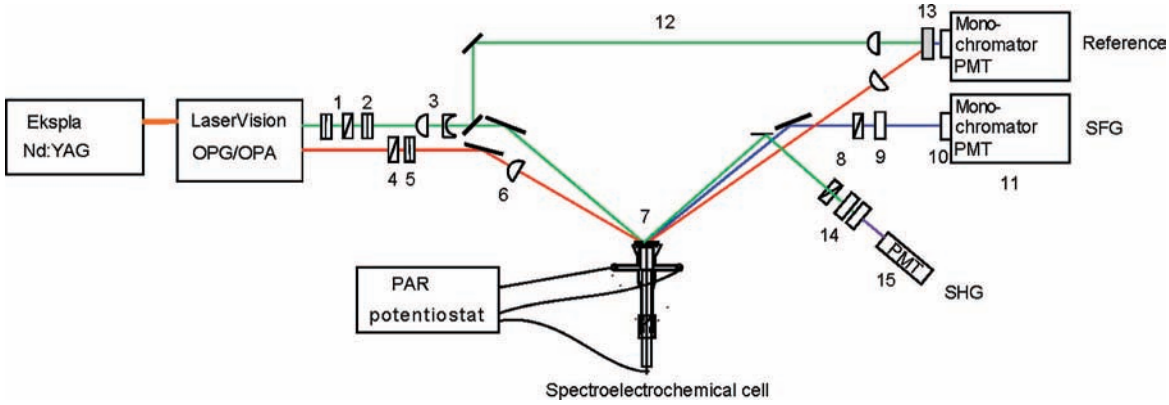


**FIGURE 3.** Diagram of the picosecond-scanning SFG spectrometer. A picosecond pulsed Nd:YAG laser (Eskpla) at 1064 nm is split into two parts. One part is frequency-doubled to 532 nm. The other part is used to pump a KTP/$AgGaSe_2$ OPG/OPA system (LaserVision) that generates infrared light (IR). Both beams are directed to the liquid sample: (1) attenuator (half-wave plates/polarizer); (2) $\lambda/2$ plate (polarization control); (3) collimating reducing telescope; (4, 5) polarizer/half-wave plate (polarization control); (6) long focal length $BaF_2$ lens (500 mm); (7) sample; (8) analysis polarizer; (9) Kaiser Notch Plus filter; (10) 515 nm short pass filter; (11) 0.25 m monochromator with PMT; (12) reference arm; (13) single-crystal quartz (nonlinear signal reference); (14) 532 nm filters; (15) PMT.

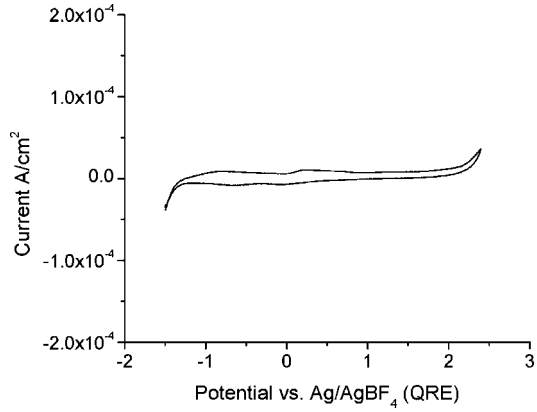


**FIGURE 4.** Cyclic voltammogram of neat [BMIM][$BF_4$] at $5 \times 10^{-5}$ Torr. Scan rate = 100 mV/s.

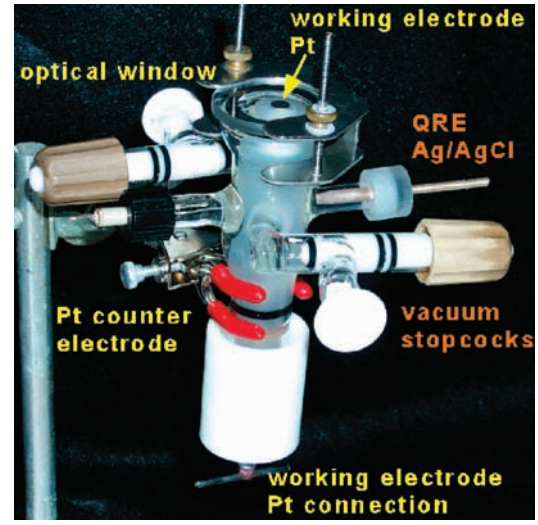


**FIGURE 5.** Thin layer SFG electrochemistry cell. Cell is able to hold vacuum down to $10^{-6}$ Torr.

development of an electrochemical cell capable of holding vacuum to $10^{-6}$ Torr to keep the ionic liquids dry and not exposed to the laboratory environment, Figure 5.

Electrochemistry provides at least three crucial roles in these experiments: control of surface charge or potential, measurement of interfacial properties through EIS and CV, and quality control on the purity of the sample.

Cyclic voltammetry is used to ensure that there are no electrochemical reactions occurring in the potential window of the experiment. Thus, all measurements are performed in the double layer region of the potential scan, where only charge and discharge of the double layer occurs. Further, the CV helps to ensure that the ionic liquid is pure since no redox processes occur due to $Cl^-$ or water. Typically $Cl^-$ is <20 ppm and water is $<10^{-4}$ mole fraction. A cyclic voltammogram is shown in Figure 4 for [BMIM][$BF_4$]. The CV also illustrates the voltage stability window from approximately 4 V. More physical information on the interface is obtained by EIS. EIS is achieved by scanning the frequency of the applied voltage (AC) and measuring the complex resistance of the cell. The system is modeled based on an equivalent electrical circuit with individual elements corresponding to different parts of the system. The values of the individual components are interpreted in terms of molecular properties. The entire EIS response is modeled based on an equivalent circuit as shown in Figure 6A. The first resistor corresponds to the solution resistance, *Q* is the dispersive capacitance related to the double layer. The lower branch in the model is the surface resistance, and *W* is the Warburg element for solution diffusion processes.[33,46,47] By fitting each EIS curve to this circuit, values of the individual elements are obtained. An example of EIS spectra at differing potentials for [BMIM][$BF_4$]/Pt is given in Figure 6B. Of interest to these studies is the capacitance of the interface and its

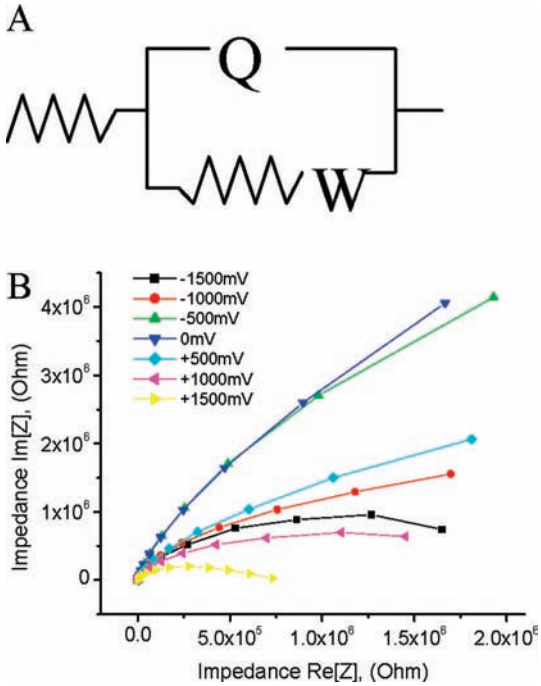


**FIGURE 6.** (A) The equivalent circuit used to model the EIS data and (B) electrochemical impedance spectra of [BMIM][$BF_4$] at the Pt electrode.

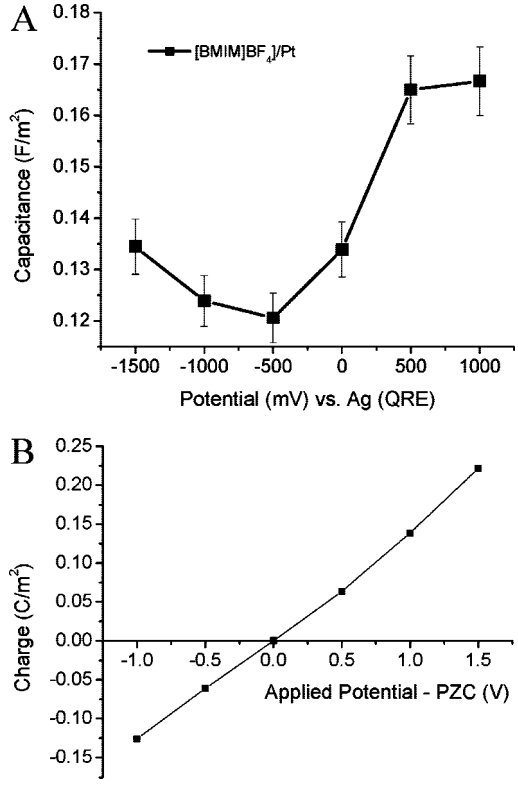


**FIGURE 7.** (A) Interfacial capacitance vs applied potential for ionic liquid [BMIM][$BF_4$] at $10^{-5}$ Torr pressure and (B) Interfacial charge vs potential from PZC.

potential dependence as displayed in Figure 7A. The curve displays a minimum at approximately −500 mV vs Ag (QRE)

**TABLE 1.** Values of Double Layer Capacitance for Room-Temperature Ionic Liquids at the Platinum Electrode

| ionic liquid $[BMIM]^+$ | capacitance ($F/m^2$) | double layer thickness (m) |
|---|---|---|
| $[PF_6]^-$ | 0.19 | $3 \times 10^{-10}$ |
| $[BF_4]^-$ | 0.12 | $5 \times 10^{-10}$ |
| $[N(CN)_2]^-$ | 0.1 | $25 \times 10^{-10}$ |
| $[imide]^-$ | 0.15 | $4 \times 10^{-10}$ |

for the [BMIM][$BF_4$]/Pt interface. This measurement has two valuable pieces of information about the interfacial structure. First, the capacitance value at the minimum is 0.12 $F/m^2$. Based on eq 1, this results in a double layer thickness of $5 \times 10^{-10}$ m or 5 Å. Second, through interpretation of the electrocapillary equation, the minimum in the capacitance–voltage curve corresponds to the potential of zero charge, PZC.[24,27,33,48,49] The analysis suggests that at potentials negative of −500 mV, the surface charge is negative, while at voltages positive of −500 mV, the surface becomes positively charged. This interpretation is based on the Gouy–Chapmann theory which, in turn, is under the same conditions as Debye–Huckel theory, the use of which is not clear when applied to the ionic liquid system.

The capacitance value implies a very thin layer at the surface. The use of a dielectric constant of $\epsilon = 7$ for the ionic liquid,[50] suggests that there is one ion layer at the electrode,

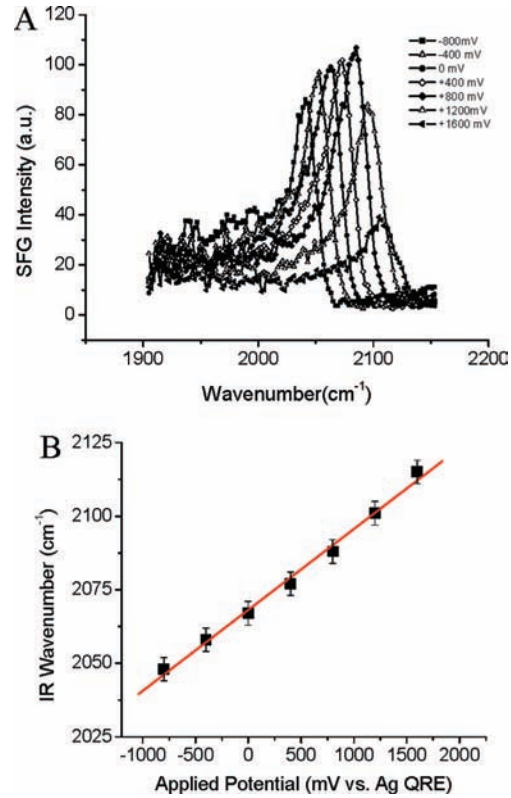


**FIGURE 8.** (A) SFG spectra of CO on Pt electrode as a function of potential, taken with ppp polarization, and (B) plot of CO peak position vs applied potential.

**TABLE 2.** Stark Shift for CO on Pt in Ionic Liquid Electrolyte

| ionic liquid $[BMIM]^+$ | Stark effect ($cm^{-1}$/V) | double layer width (m) |
|---|---|---|
| $[PF_6]^-$ | 26 | $3.8 \times 10^{-10}$ |
| $[BF_4]^-$ | 33 | $3.3 \times 10^{-10}$ |
| $[imide]^-$ | 24 | $4.2 \times 10^{-10}$ |
| [DCA]- | <10 | $25 \times 10^{-10}$ |

which screens the surface charge such that the potential drop is complete, and beyond this distance, the ionic liquid adopts essentially the bulk structure. Table 1 contains the capacitance and thickness values for other room-temperature ionic liquids and indicates a similar though ion-dependent structure.

The potential drop across the interface is directly measured by the use of probe molecules. Carbon monoxide displays a dramatic shift in its vibrational frequency as a function of the external electric field known as the vibrational Stark effect.[51,52] To observe this effect, CO is adsorbed to the Pt electrode through the carbon atom.[53] Again, the description is as follows: the Pt electrode is one plate of the parallel plate capacitor model and the transition from double layer to bulk liquid is the other "plate". The SFG spectra in Figure 8A show a single C≡O stretch peak near 2100 $cm^{-1}$. The peak shifts from 2045 $cm^{-1}$ at low potential to 2110 $cm^{-1}$ at high potential for a Stark shift tuning rate, $d\nu/d\varphi$, of 33 $cm^{-1}$/V for $[BMIM][BF_4]$. (Figure 8B) The Stark shift tuning rate for other ionic liquids is given in Table 2. The absolute Stark shift for CO $d\nu_{CO}/dE_{loc}$ is $1 \times 10^{-6}$ V/cm.[51] Thus, the double layer thickness is estimated to be $d\nu_{CO}/dE_{loc}^{TM}\, d\nu/d\varphi = 3.3 \times 10^{-10}$ m. That is, the electric field across the interface results in a Stark shift for CO and corresponds to an equivalent capacitor thickness of 3−4 Å, Figure 9. These two independent measurements, vibrational Stark shift and capacitance, suggest that the ionic liquid−metal interface is one ion-layer thick; essentially a Helmholtz layer.[54]

Establishing the thickness of the interfacial region is important in analyzing the SFG data. Although SFG is surface sensitive, it detects multiple layers if the molecules or ions reside in a noncentrosymmetric environment. Establishing that ionic liquids form essentially one layer allows for a more straightforward analysis of the SFG data.

A SFG spectrum of $[BMIM]^+$ at the Pt electrode and number scheme are shown in Figure 10. The spectrum displays several resonances in the C−H stretching region. The symmetric and asymmetric $CH_2$ modes are at 2850 and 2915 $cm^{-1}$, respectively.[55] Methyl group vibrations of the butyl chain are at 2875, 2930, and 2965 $cm^{-1}$,[55,56] while the N(3)−$CH_3$ methyl symmetric stretch is at 2945 $cm^{-1}$.[57] Above 3000 $cm^{-1}$ are resonances due to the aromatic C−H stretches such as C(2)−H at 3050 $cm^{-1}$ and H−C(4)C(5)−H between 3150 and 3190 $cm^{-1}$.[58,59] All these peaks are superimposed on a large nonresonant background signal of the charged Pt electrode. The dashed line in the spectrum is a fit according to eq 5. The following analysis focuses on the 3190 $cm^{-1}$ peak, the H−C(4)C(5)−H symmetric stretch. This is due to rel-

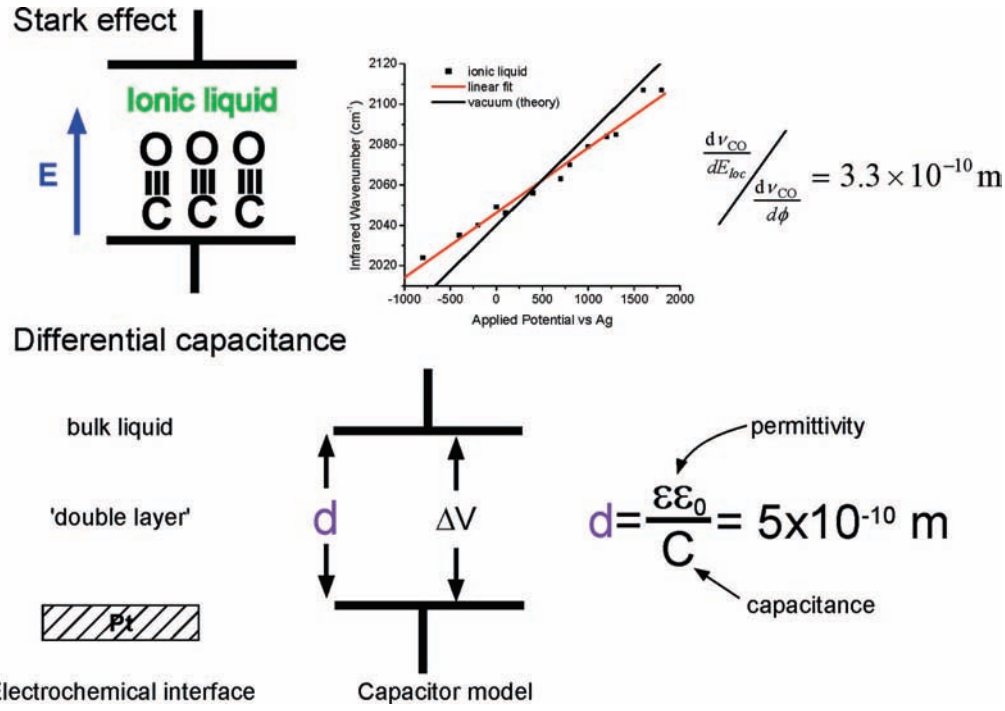


**FIGURE 9.** A summary of two different views on the thickness of the interfacial layer between ionic liquid and metal electrode: top, vibrational Stark shift measurement; bottom, double layer capacitance.

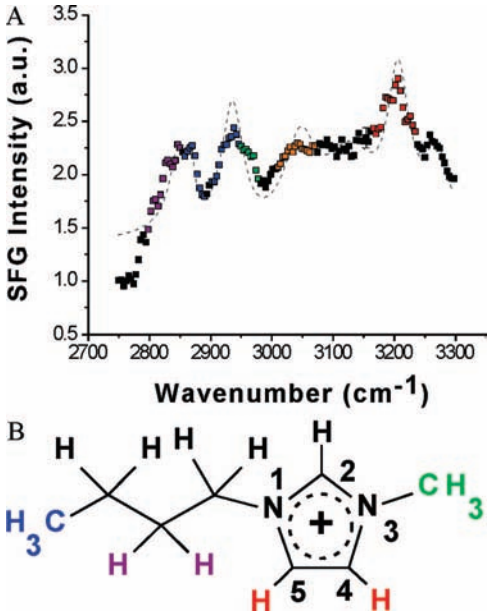


**FIGURE 10.** (A) SFG spectrum of $[BMIM]^+$ at the Pt electrode with ppp polarization and (B) Structure of $[BMIM]^+$ cation with color code and number scheme. Color corresponds to the colored region in the SFG spectrum in part A.

atively large signal free of spectral interference from other modes. Also, since the interfacial model deals with a charged metal interface and the charge on imidazolium is centered on the aromatic ring, the H−C(4)C(5)−H vibration is a good reporter on how the surface charge influences the interfacial arrangement of the ionic liquid.

To deduce how the surface charge and potential influence the structure of the ionic liquid, SFG spectra are obtained in two polarization combinations, ssp and ppp (SF, visible, and IR, respectively). By taking the peak intensity ratio from the two polarizations, an estimate of the functional group orientation is obtained.[60] Polarization- and potential-dependent SFG spectra are shown in Figure 11. Thus, the influence of surface potential (or charge) on the orientation of the imidazolium ring is measured and correlated to the results of the electrochemical measurements.[61]

SFG results also indicate that both cations and anions are oriented at the surface as seen the SFG spectra for dicyanamide, $[DCA]^-$, in Figure 12. The large increase in SFG signal is observed upon going from −400 to +800 mV. This peak at ~2160 $cm^{-1}$ is due to the C≡N symmetric stretch.[62]

The results suggest that both ions are oriented at the surface and that SFG signal from the anion grows stronger at positive surface charge while the cation signal is related to the negative surface charge. The results of the polarization- and potential-dependent SFG analysis are presented in Figure 13.

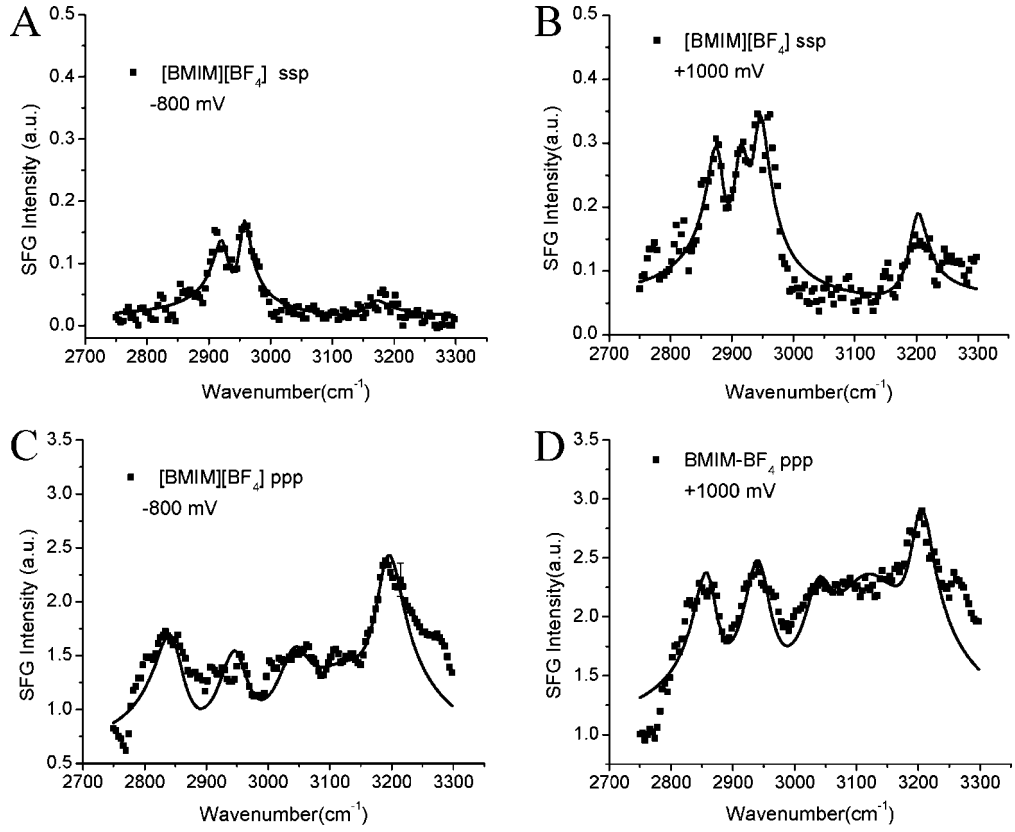


**FIGURE 11.** SFG spectra of $[BMIM]^+$ at the Pt electrode taken at two different polarization combinations and two potentials: (A) ssp at −800 mV; (B) ssp at $^+$1000 mV; (C) ppp at −800 mV; (D) ppp at +1000 mV.

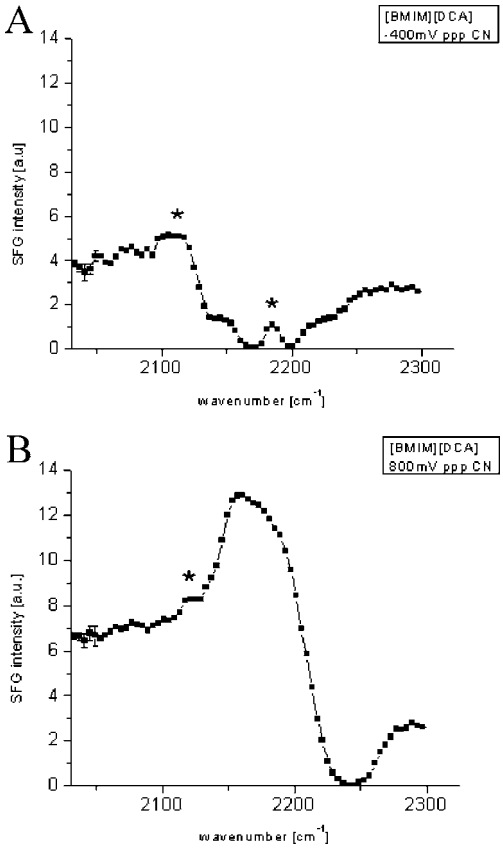


**FIGURE 12.** SFG spectra of $[DCA]^-$ at the Pt electrode taken at ppp polarization and two potentials: (A) −400 mV; (B) +800 mV.

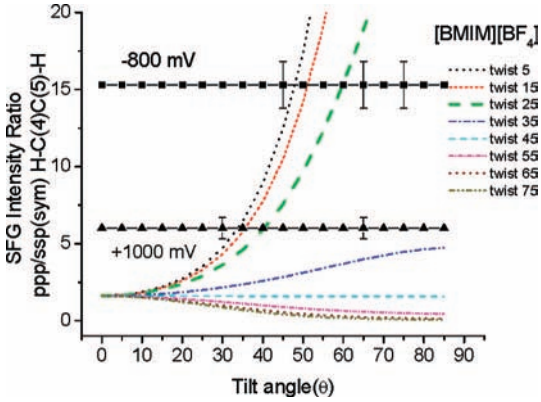


**FIGURE 13.** Orientation plots for the H−C(4)C(5)−H symmetric stretch as orientation tilt angle vs SFG intensity ratio. Each curve is for a different twist angle about the $C_2$ axis.

The figure displays the intensity ratio of the H−C(4)C(5)−H symmetric stretch from the ppp/ssp spectra vs tilt orientation, $\theta$, along the surface normal. The H−C(4)C(5)−H mode is approximately $C_{2v}$ symmetry and therefore, needs both tilt ($\theta$) and twist ($\varphi$) angles to describe the orientation at the surface. Tilt is along the surface normal, while twist is around the pseudo-$C_2$ axis. The plots in Figure 13 show the results of the simulation of the SFG signal for varying orientations of the imidazolium ring. A tilt angle of 0° had the ring perpendicular to the surface plane, that is $C_2$ axis along the surface normal. A twist of 0° has the ring plane cofacial with the surface plane, while at $\varphi = 90°$, the ring is perpendicular to the surface plane, that is, $C_2$ axis parallel to the surface plane, see Figure 14.

The solid black line in Figure 13 is the measured ratio at two potentials, −800 and +1000 mV. From the intersection of the simulation curves to the experimental measurement, it is seen that for a positive surface potential of +1000 mV, the ring is oriented mostly along the surface normal, while as the potential is scanned to a more negative value, the ring becomes aligned more parallel to the surface plane. A schematic of this process is shown in Figure 14.

The orientation result is understood in terms of the electrochemical results of interfacial capacitance, Figure 7A, where at potential less than −500 mV (PZC) the surface has a negative charge and at potential positive of PZC it has a positive charge. Consequently, at a positive surface charge, the cation ring is repelled from the Pt surface and caused to tilt more along the surface normal. Similarly, this allows more room for the anion, $[BF_4]^-$, to have more access to the surface to screen the positive charge. However, at negative surface charge, the ring is attracted to the surface and adopts a more parallel orientation to the surface plane. A similar model is postulated for [BMIM][$PF_6$],[61] [BMIM][imide], and [BMIM][I].

The results of this project on the structure of room-temperature ionic liquids at the electrified interface have been both enlightening and puzzling. First it has been demonstrated that the interfacial region is one ion layer thick. This result was based on the interfacial capacitance and the vibrational Stark shift of CO at the interface. The results are understood by considering at the high charge density of the ionic liquid that the surface fields are sufficiently screened after one layer of ions. While this result could be anticipated by Gouy–Chapmann theory, in the limit of infinite electrolyte concentration, for pure ions, the double layer shrinks to zero. The same interpretation is derived from Debye–Huckel theory.[63] However, these theories are presumably no longer valid in such high ion concentration as in the ionic liquid since they are valid in the limit of infinite dilution. Further, the one ion-layer model is not obvious considering that research on molten salts adjacent to the electrode suggests a multilayer structure.[23,28–30,32] The multilayer model is not observed for these room temperature ionic liquids, save possibly [BMIM][DCA], see above.

Also SFG has demonstrated that an oriented layer of ions does exist at the electrode interface and that the orientation depends on the surface charge. The influence of the electrode surface is, in a first-order approximation, understood based on

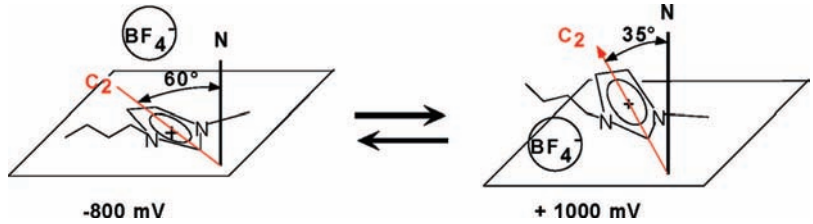


**FIGURE 14.** Representation of the orientation of $[BMIM]^+$ on the surface of the Pt electrode.

electrostatic principles. The surface of the metal is considered as a smooth, homogeneous slab of charge, where the metal identity is of secondary importance. As the surface charge is made negative, the imidazolium ring, where the positive charge is centered, lies more parallel to the surface to maximize the attractive interaction. Likewise, as the surface becomes more positively charged, the imidazolium ring is repelled from the surface, and the anion is now interacting with the Pt surface to screen the positive charge. The cation responds to this by getting out of the way, that is, tilting along the surface normal to make room for the anion.

Further, there appears to be subtle differences in the interfacial structure and ion response to surface charge that depend on the ions that make up the ionic liquid. For example, upon comparison of $[BMIM][BF_4]$ to $[BMIM][PF_6]$, the imidazolium ring of the latter appears to twist about the $C_2$ axis to allow the $[PF_6]^-$ access to the Pt surface, while in the former case, the ring tilted.[61] The difference is subtle but could be linked to the different size or symmetry of the anion. Similarly, when ions such as $[BF_4]^-$, $[PF_6]^-$, or $[imide]^-$ are substituted with $[DCA]^-$, the interfacial structure extends from about one layer to approximately five layers. The coordinating ability of $[DCA]^-$ may be responsible for this. While many interface properties of ionic liquids have been discovered in this research, several fundamental questions have also been raised.

1. If room-temperature ionic liquids form essentially a Helmholtz layer at the interface, why does the $C-V$ curve display a minimum? This should only happen in the presence of a diffuse layer such as in the Gouy–Chapman model.
2. Is the capacitance minimum at the PZC? If so, why? This system is not a dilute electrolyte; therefore Debye–Huckel or Gouy–Chapmann limiting laws should not apply.
3. On each side of the capacitance minimum there should be excess positive or negative charge accumulation, according to Gouy–Chapmann. How is this possible in a pure electrolyte? It is difficult to envision that the classic PZC, where the concentration of ions at the surface is the same as that in the bulk electrolyte, applies to the ionic liquids.
4. Is the ionic liquid in contact with the metal similar to having specific adsorption from solution?

Very little work has been presented on the structure of ionic liquids near a charged interface. Earlier theoretical calculations and simulations were on molten salts; however they may not be appropriate for these new room-temperature ionic liquids, since these ions have shape and other interactions that affect their arrangement at the interface.[28−30] Recent calculations on molten salts have been more successful at reproducing the electrochemical data.[31,47] However, these compounds, room-temperature ionic liquids, will require more research to fully understand their nature. Recently, work by Madden et al. indicated a single layer of screening charge at the molten salt interface,[64] somewhat in line with the SFG and electrochemical measurements presented here. The results of surface charge vs potential from PZC are shown in Figure 7B. In a simple case, one monolayer of charge is 0.26 C/m$^2$. As noted previously, the capacitance suggests that at PZC (−500 mV), there exists a layer of ions, thus, in order to create the next layer of ions the potential must be ±1500 mV from PZC (see Figure 7B).

Finally, there have been two recent theoretical works on the interfacial structure of ionic liquids near a charged surface. The work of Lynden-Bell has been very important in this direction,[65] where some of the results coincide with the results of our experimental work, especially the ion orientation in the first layer and the surface excess. Similarly, the work of Kornyshev is enlightening and important in recognizing that using the classic double layer theories applied to ionic liquids is not yet justified on theoretical grounds.[66] It is interesting to point out that the theory of ion/electrical transport in ionic liquids is described in terms of holes (vacancies) in the liquid structure.[67,68] Thus, holes are the dilute species in a solvent of charges; perhaps this is analogous to the Debye–Huckel limiting law.

Electrochemical interfaces involving ionic liquids are a new challenge to the surface chemist, electrochemist, and theoretician. With new models and new experimental techniques, the details of this important system should be uncovered.

*I would like to thank the R. A. Welch Foundation and ACS-PRF for support of this research. I also thank Selimar Rivera, Casey Romero, Cesar Aliaga, and Cherry Santos on their exceptional work on the surface chemistry of ionic liquids.*

## BIOGRAPHICAL INFORMATION

**Steve Baldelli** received his B.S. degree from Framingham State College in Massachusetts in 1992 and his Ph.D. from Tufts University in 1998 under the direction of Mary Shultz. After spending three years at the University of California, Berkeley, with Gabor Somorjai and Phil Ross, he moved to University of Houston, where he is now an associate professor of chemistry. He is also a visiting professor at the Royal Institute of Technology in Stockholm, Sweden. His interests center on using linear and nonlinear spectroscopic and microscopic methods to study surface chemistry problems including liquid and solid interfaces, SAMs, electrochemical interfaces, and problems in corrosion.

## REFERENCES


1 Hagiwara, R. Ionic liquids. *Electrochemistry* **2002**, *70*, 130–135.

2 Hussey, C. L. In *Chemistry of Nonaqueous Solutions*; Mamantov, G., Popov, A. I., Eds.; VCH: New York, 1994; p 376.

3 Tsuda, T.; Hussey, C. L. Electrochemical applications of room-temperature ionic liquids. *Interface* **2007**, *16*, 42–49.

4 Koch, V. R.; Dominey, L. A.; Nanjundiah, C.; Ondrechen, M. J. The intrinsic anodic stability of several anions comprising solvent-free ionic liquids. *J. Electrochem. Soc.* **1996**, *143*, 798–803.

5 Matsumoto, K.; Hagiwara, H.; Ito, Y. Room-temperature ionic liquids with high conductivities and wide electrochemical windows. *Electrochem. Solid-State Lett.* **2004**, *7*, E41–E47.

6 de Souza, R.; Padilha, J. C.; Gonc, R. S.; Dupont, J. Room temperature dialkylimidazolium ionic liquid-based fuel cells. *Electrochem. Commun.* **2003**, *5*, 728–731.

7 Nakamoto, H.; Noda, A.; Hayamizu, K.; Hayashi, S.; Hamaguchi, H.; Watanabe, M. Proton-conducting properties of a bronsted acid-base ionic liquid and ionic melts consisting of bis. (trifluoromethanesulfonyl)imide and benzimidazole for fuel cell electrolytes. *J. Phys. Chem. C.* **2007**, *111*, 1541–1548.

8 Noda, A.; Susan, A. B.; Kudo, K.; Mitsushima, S.; Hayamizu, K.; Watanabe, M. Bronsted acid-base ionic liquids as proton-conducting nonaqueous electrolytes. *J. Phys. Chem. B* **2003**, *107*, 4024–4033.

9 Balducci, A.; Bardi, U.; Caporali, S.; Mastragostino, M.; Soavi, F. Ionic liquids for hybrid supercapacitors. *Electrochem. Commun.* **2004**, *6*, 566–568.

10 Nanjundiah, C.; McDevitt, S. F.; Koch, V. R. Differential capacitance measurements in solvent-free ionic liquids at Hg and C interfaces. *J. Electrochem. Soc.* **1997**, *144*, 3392–3397.

11 Ue, M.; Takeda, T.; Takahashi, T.; Takehara, M. Ionic liquids with low melting points and their application to double-layer capacitor electrolytes. *Electrochem. Solid-State Lett.* **2002**, *5*, A119–A121.

12 Kawano, R.; Watanabe, M. Equilibrium potentials and charge transport of an I-/I3- redox couple in an ionic liquid. *Chem. Commun.* **2003**, 330–332.

13 Papageorgiou, N.; Athanassov, Y.; Armand, M.; Bonhôte, P.; Pettersson, H.; Azam, A.; Grätzel, M. The performance and stabilty of ambient temperature molten salts for solar cell applications. *J. Electrochem. Soc.* **1996**, *143*, 3099–3108.

14 Wang, P.; Zakeeruddin, S.; Moser, J.; Gratzel, M. A new electrolyte enhances the conversion efficiency of dye-sensitized solar cells. *J. Phys. Chem. B* **2003**, *107*, 13280–13285.

15 Yamanaka, N.; Kawano, R.; Kubo, W.; Masaki, N.; Kitamura, T.; Wada, Y.; Watanabe, M.; Yanagida, S. Dye-sensitized $TiO_2$ solar cells using imidazolium-type ionic liquid crystal systems as effective electrolytes. *J. Phys. Chem. B.* **2007**, *111*, 4763–4769.

16 Lu, W.; Fadeev, A. G.; Qi, B.; Smela, E.; Mattes, B. R.; Ding, J.; Spinks, G. M.; Mazurkiewicz, J.; Zhou, D.; Wallace, G. G.; MacFarlane, D. R.; Forsyth, M.; Forsyth, S. A. Use of ionic liquids for pi-conjugated polymer electrochemical devices. *Science* **2002**, *297*, 983–987.

17 Pernak, J.; Czepukowicz, A.; Pozniak, R. New ionic liquids and their antielectrostatic properties. *Ind. Eng. Chem. Res.* **2001**, *40*, 2379–2383.

18 Endres, F. Electrodeposition of a thin germanium film on gold from a room temperature ionic liquid. *Phys. Chem. Chem. Phys.* **2001**, *3*, 3165–3174.

19 Murakami, T.; Nishikiori, T.; Nohira, T.; Ito, Y. Electrolytic synthesis of ammonia in molten salts under atmospheric pressure. *J. Am. Chem. Soc.* **2003**, *125*, 334–335.

20 Welton, T. Room-temperature ionic liquids. Solvents for synthesis and catalysis. *Chem. Rev.* **1999**, *99*, 2071–2083.

21 Tokuda, H.; Hayamizu, K.; Ishii, K.; Susan, M.; Watanabe, M. Physicochemical properties and structures of room temperature ionic liquids. 2. Variation of alkyl chain length in imidazolium cation. *J. Phys. Chem. B* **2005**, *109*, 6103–6111.

22 Tokuda, H.; Hayamizu, K.; Ishii, K.; Susan, M.; Watanabe, M. Physicochemical properties and structures of room temperature ionic liquids. 1. Variation of anionic species. *J. Phys. Chem. B* **2004**, *108*, 16593–16601.

23 Devanathan, M. A.; Tilak, B. V. The structure of the electrical double layer at the metal–solution interface. *Chem. Rev.* **1965**, *65*, 635–680.

24 Grahame, D. C. The electrical double layer and the theory of electrocapillarity. *Chem. Rev.* **1947**, *41*, 441–501.

25 Parsons, R. Electrical double layer: Recent experimental and theoretical developments. *Chem. Rev.* **1990**, *90*, 813–826.

26 Sparnaay, M. J. *The Electrical Double Layer*; Pergamon: New York, 1972.

27 Bockris, J. O.; Reddy, A. K. N. *Modern Electrochemistry: Fundamentals of Electrodics*; 2nd ed.; Kluwer/Plenum Press: New York, 1998; Vol. 2.

28 Graves, A. D. The electrical double layer in molten salts. Part 1. The potential of zero charge. *Electroanal. Chem.* **1970**, *25*, 349–356.

29 Graves, A. D.; Inman, D. The electrical double layer in molten salts. Part 2. The double layer capacitance. *Electroanal. Chem.* **1970**, *25*, 357–372.

30 Sotnikov, A. I.; Esin, O. A. *Phys. Chem. Electrochem. Molten Salts Slags, 3rd All Soviet Conf.: Lenningrad* **1966**, 209–214.

31 Kisza, A. The capacitance of the electric double layer of electrodes in molten salts. *J. Electroanal. Chem.* **2002**, *534*, 99–106.

32 Inman, D.; Lovering, D. G. In *Comprehensive Treatise of Electrochemistry*; Conway, B. E., Bockris, J. O., Yeager, E., Khan, S. U., White, R. E., Eds.; Plenum: New York, 1983; Vol. 7; p 593.

33 Bard, A. J.; Faulkner, L. R. *Electrochemical Methods*; 2nd ed.; John Wiley and Sons: New York, 2001.

34 Baldelli, S.; Gewirth, A. A. In *Advances in Electrochemistry*; Ross, P. N., Lipkowski, J., Eds.; Wiley: New York, 2007; Vol. 11.

35 Guyot-Sionnest, P.; Tadjeddine, A. Spectroscopic investigations of adsorbates at the metal-electrolyte interface using sum frequency generation. *Chem. Phys. Lett.* **1990**, *172*, 341–345.

36 Tadjeddine, A.; LeRille, A.; Pluchery, O.; Vidal, F.; Zheng, W. Q.; Peremans, A. Sum and difference frequency generation at the electrochemical interface. *Phys. Status Solidi A* **1999**, *175*, 89–98.

37 Huang, J. Y.; Shen, Y. R. In *Laser Spectroscopy and Photochemistry on Metal Surfaces*; Dai, H. L., Ho, W., Eds.; World Scientific: Singapore, 1995.

38 Bain, C. D. Sum frequency vibrational spectroscopy of the solid/liquid interface. *J. Chem. Soc., Faraday Trans.* **1995**, *91*, 1281–1292.

39 Matranga, C.; Wehrenberg, B. L.; Guyot-Sionnest, P. Vibrational relaxation of cyanide on copper surfaces: Can metal d-bands influence vibrational energy transfer. *J. Phys. Chem. B* **2002**, *106*, 8172–8178.

40 Kuhnke, K.; Morin, M.; Jakob, P.; Levinos, N. J.; Chabal, Y. J.; Harris, A. L. Vibrational energy transfer among adsorbate modes: Picosecond dynamics on stepped H/Si(111). *J. Chem. Phys.* **1993**, *99*, 6114–6121.

41 Cimatu, K. A.; Baldelli, S. Sum frequency generation microscopy of microcontact-printed mixed self-assembled monolayers. *J. Phys. Chem. B* **2006**, *110*, 1807–1813.

42 Cimatu, K. A.; Baldelli, S. Sum frequency generation imaging of CO on platinum surfaces. *J. Am. Chem. Soc.* **2006**, *128*, 16016–16017.

43 Cimatu, K. A.; Baldelli, S. Spatial surface analysis of octadecanethiol self-assembled monolayers on mild steel using the sum frequency generation imaging microscope. *J. Phys. Chem. C* **2007**, *111*, 7137–7143.

44 Cimatu, K. A.; Moore, H. J.; Lee, T. R.; Baldelli, S. Sum frequency generation imaging of microcontact-printed monolayers derived from aliphatic dithiocarboxylic acids: Contrast based on terminal group orientation. *J. Phys. Chem. C* **2007**, *111*, 11751–11755.

45 Baldelli, S. Influence of water on the orientation of cations at the surface of a room temperature ionic liquid studied with sum frequency generation vibrational spectroscopy. *J. Phys. Chem. B* **2003**, *107*, 6148–6152.

46 Popova, A.; Raicheva, S.; Sokolova, E.; Christov, M. Frequency dispersion of the interfacial impedance at mild steel corrosion in mild acid media in the presence of benzimidazole derivatives. *Langmuir* **1996**, *12*, 2083–2089.

47 Kisza, A. The capacitance of the diffuse layer of electric double layer of electrodes in molten salts. *Electrochim. Acta* **2006**, 2315–2321.

48 Bockris, J. O.; Reddy, A. K. N. *Modern Electrochemistry: Ionics*; 2nd ed.; Plenum Press: New York, 1998; Vol. 1.

49 Grahame, D. C. Effects of dielectric saturation upon the diffuse double layer and the free energy of hydration of ions. *J. Chem. Phys.* **1950**, *18*, 903–912.

50 Daguenet, C.; Dyson, P. J.; Krossing, I.; Oleinikova, A.; Slattery, J.; Wakai, C.; Weingartner, H. Dielectric responce of imidazolium-based room-temperature ionic liquids. *J. Phys. Chem. B* **2006**, *110*, 12682–12688.

51 Lambert, D. K. Vibrational stark effect of adsorbates at electrochemical interfaces. *Electrochim. Acta* **1996**, *41*, 623–630.

52 Lambert, D. K. Vibrational Stark effect of CO on Ni(100), and CO in the aqueous double layer: Experiment, theory, and models. *J. Chem. Phys.* **1988**, *89*, 3847–3860.

53 Blyholder, G. Molecular orbital view of chemisorbed carbon monoxide. *J. Phys. Chem.* **1964**, *68*, 2772–2777.

54 Baldelli, S. Probing electric fields at the ionic liquid-electrode interface using sum frequency generation spectroscopy and electrochemistry. *J. Phys. Chem. B* **2005**, *109*, 13049–13051.

55 Snyder, R. G.; Strauss, H. L.; Elliger, C. A. C-H stretching modes and the structure of n-alkyl chains. 1. Long, disordered chains. *J. Phys. Chem.* **1982**, *86*, 5145–5150.

56 MacPhail, R. A.; Strauss, H. L.; Snyder, R. G.; Elliger, C. A. C-H stretching modes and the structure on n-alkyl chains. 2. Long, all-trans chains. *J. Phys. Chem.* **1984**, *88*, 334–341.

57 Rivera-Rubero, S.; Baldelli, S. Surface characterization of 1-butyl-3-methylimidazolium-based ionic liquids, [BMIM][X], X = $Br^-$, $I^-$, $PF_6^-$, $BF_4^-$, $(CF_3SO_2)_2N^-$, $SCN^-$, $CH_3SO_3^-$, $CH_3SO_4^-$, or $(CN)_2N^-$ by sum frequency generation vibrational spectroscopy. *J. Phys. Chem. B* **2006**, *110*, 4756–4765.

58 Tait, S.; Osteryoung, R. A. Infrared study of ambient-temperature chloroaluminates as a function of melt acidity. *Inorg. Chem.* **1984**, *23*, 4352–4360.

59 Talaty, E. R.; Raja, S.; Storhaug, V. J.; Dolle, A.; Carper, W. R. Raman and infrared spectra and ab initio calculations of $C_{2-4}$MIM imidazolium hexaflurophosphate ionic liquids. *J. Phys. Chem. B* **2004**, *108*, 13177–13184.

60 Wang, H. F.; Gan, W.; Lu, R.; Rao, Y.; Wu, B. H. Quantitiative spectral and orientational analysis in surface sum frequency generation vibrational spectroscopy (SFG-VS). *Int. Rev. Phys. Chem.* **2005**, *24*, 191–257.

61 Rivera-Rubero, S.; Baldelli, S. Surface spectroscopy of room-temperature ionic liquids on a platinum electrode: A sum frequency generation study. *J. Phys. Chem. B* **2004**, *108*, 15133–15140.

62 Dahl, K.; Sando, G. M.; Fox, D. M.; Sutto, T. E.; Owrutsky, J. C. Vibrational spectroscopy and dynamics of small anions in ionic liquid solutions. *J. Chem. Phys.* **2005**, *123*, 084504.

63 Lewis, G. N.; Randall, M. *Thermodynamics*; McGraw-Hill: New York, 1961.

64 Lanning, O. J.; Madden, P. A. Screening at a charged surface by a molten salt. *J. Phys. Chem. B* **2004**, *108*, 11069–11072.

65 Pinilla, C.; Popolo, M. G.; Kohanoff, J.; Lynden-Bell, R. M. Polarization relaxation in a ionic liquid confined between electrified walls. *J. Phys. Chem. B* **2007**, *111*, 4877–4884.

66 Kornyshev, A. A. Double-layer in ionic liquids: Paradigm change. *J. Phys. Chem. B* **2007**, *111*, 5545–5558.

67 Bockris, J. O.; Reddy, A. K. N. *Modern Electrochemistry*; 2nd ed.; Kluwer/Plenum: New York, 1998; Vol. 2.

68 Abbott, A. P. Model for the conductivity of ionic liquids based on an infinite dilution of holes. *Chem. Phys. Chem.* **2005**, *6*, 2502–2508.